ORIGINAL RESEARCH ARTICLE

Decarburization and Gas Formation During Sintering of Alloyed PM Steel Components

PETER QUADBECK, ALEXANDER STRAUß, and THOMAS WEIßGÄRBER

This study investigates the delubrication, reduction, and decarburization processes of powder metallurgical steel alloys (CrM, CrL, AHC, Mo85, SintD 35) and an unalloyed steel during sintering in a pure hydrogen atmosphere. Utilizing in-situ FTIR gas phase analysis, components with ethylenebisstearamide (EBS) as a lubricant are analyzed. EBS decomposition in steel components yields CO, CO_2, H_2O, and CH_4, with dominant CH groups observed in the 230 °C to 480 °C range. In the temperature range between 750 °C and 850 °C, where CO formation is expected due to the reduction of surface iron oxides, CH_4 is present instead, indicating that an ''internal getter effect'' also occurs in pre-alloyed powders. In addition, with high carbon activity, the reduction of internal iron oxides and the reduction of chromium oxides also trigger an internal getter effect. Depending on the carbon potential, these processes cause a considerable reduction in the carbon content of the powder metallurgical components. The study therefore shows that the decarburization of powder metallurgical components during the heat treatment phases prior to sintering in a 100 pct hydrogen atmosphere is less due to the mechanism of delubrication, but rather to mechanisms of carbothermal reduction.

https://doi.org/10.1007/s11663-024-03237-5
© The Author(s) 2024

I. INTRODUCTION

SINTERING of PM steel components is subject to manifold processes which occur during the initial stage of the heat treatment prior to sintering. Beyond drying, the decomposition of the lubricants, reduction processes of surface powder particle oxides as well as carburization or decarburization processes occur. These initial steps are crucial for the final sintering step and for the properties of the sintered product. As an example, the reduction of the oxide scales on the particle surfaces on the one hand is essential in order to allow the sintering necks between the particles to grow since the oxides suppress the sinter activity. Carbon control, on the other hand, is needed since the strength, hardness, corrosion resistance, and hardenability are significantly affected by the carbon content.[1] However, it has been shown that the contribution of the allowed carbon range to the scattering of properties is comparable to the contribution of density.[2] A comparison between conventional steels and PM steels shows strongly differing carbon content tolerances. Thus, proper PM manufacturing needs proper control of all heat treatment steps prior to sintering.

One of the first steps of the heat treatment is the debinding process of the lubricants and additives. The fundamentals of thermal decomposition of such polymers were investigated in earlier studies.[3] Polymers undergo a variety of intrinsic degradation processes during thermolysis, including depolymerization, random scission, and side group elimination. In this way, easily decomposable volatile degradation products are formed on one hand; on the other hand, side reactions such as cyclization and cross-linking create thermally stable compounds, which lead to the formation of residual carbon.[4]

A typical lubricant that is used in powder metallurgy is ethylenebisstearamide (EBS, $C_{38}H_{76}N_2O_2$). Basically, the polymer consists of a dimer with two long-chain aliphatic hydrocarbons and two functional carboxylic groups, which are connected by an ethyl group. The decomposition of EBS molecules can occur *via* several competitive pathways. Baum *et al.* postulate two relevant pathways during the delubrication of Fe/EBS compacts in N_2H_2 atmosphere: firstly, decomposition into smaller fragments occurs through decarboxylation, releasing CO_2. Secondly, the predominant part of the

PETER QUADBECK is with the Offenburg University of Applied Sciences, Badstraße 24, 77652 Offenburg, Germany. Contact e-mail: peter.quadbeck@hs-offenburg.de ALEXANDER STRAUß is with the Fraunhofer Institute for Manufacturing Technology and Advanced Materials IFAM, Branch Lab Dresden, Winterbergstraße 28, 01277 Dresden, Germany. THOMAS WEIßGÄRBER is with the Fraunhofer Institute for Manufacturing Technology and Advanced Materials IFAM and also with the Dresden University of Technology, Mommsenstraße 13, 01062 Dresden, Germany.

Manuscript submitted February 28, 2024; accepted August 1, 2024.

Published online: 27 August 2024

molecule decomposes through cis-elimination, wherein characteristic features such as the CH out-of-plane wagging of the vinyl group, the vinyl C=C stretch, and the *N*-vinyl amide carbonyl stretch are observed.[5] The cis-elimination is a process in which functional groups on adjacent carbon atoms of the same side in an organic compound are eliminated. This process results in structural changes in the molecule, particularly the formation of a double bond and the release of molecular fragments. Such decomposition mechanisms occur in the temperature range of 400 °C to 700 °C. If significantly higher temperatures are applied during delubrication, the carbon content of the components is reduced, but on the other hand leads to the formation of very stable oxides, particularly in alloyed steels.[6]

In addition to the decomposition of the molecular chains of the lubricants, reduction and decarburization play a particularly important role prior to sintering. In general, powder metallurgical components are reduced by hydrogenation or carbothermal reduction. This is the case for unalloyed and for alloyed components as well. Hydrogenation requires a hydrogen-containing atmosphere and typically takes place at 300 °C to 580 °C,[7] depending on the water content in the protective gas.

A carbothermal reduction under an inert atmosphere occurs primarily through

$$\mathrm{Me}_n\mathrm{O}_m + m\mathrm{C} \leftrightarrow n\mathrm{Me} + m\mathrm{CO}. \quad [1]$$

This means that carbothermal reduction under these conditions can be measured by CO formation. As an example, the equilibrium of the reduction of iron by $Fe_2O_3 + 3C \leftrightarrow 2Fe + 3CO$ is on the right side at temperatures above 685 °C. Such peaks of CO formation under inert atmosphere are shown in the temperature range of 700 °C to 760 °C.[7,9] In addition, Oro *et al.* also report a gradual reduction of $Fe_2O_3 \rightarrow Fe_3O_4$ at 900 °C, $Fe_3O_4 \rightarrow FeO$ at 1020 °C to 1030 °C, and $FeO \rightarrow Fe$ at 1050 °C.[10] In other work, the typically very prominent release of CO in the < 1050 °C range is identified with the reduction of internal oxides.[7–9]

In addition, the carbothermal reduction of the alloying elements has been studied as well. As an example, Fe3Cr1.0C components show pronounced CO formation at 850 °C. Hryha *et al.* attribute these CO formation peaks to the reduction of internal iron oxides and surface chromium oxides.[8] Here, in the initial stages of deoxidation, the spinel oxide $FeCr_2O_4$ is carbothermally reduced. Furthermore, Astaloy CrM components exhibit weak CO peaks at 600 °C, 800 °C[9] and more intense maxima between 950 °C and 1150 °C.[7] Mori *et al.* proposed that the reduction at the initial stage of the reduction is dominated by the direct reaction of the oxides with small graphite particles.[11] Finally, the reduction of chromium oxides with spontaneous CO formation at 1136 °C has been shown in Reference 10. More stable are oxides formed by manganese, often used as strengthening element. Much like chromium, in the initial stages of the reduction, manganese forms the spinel oxide $MnFe_2O_4$. The reduction of MnO then is indicated by CO formation at temperatures above 1100 °C.[8]

Under a pure hydrogen atmosphere, the release of methane in particular is detected in addition to the species mentioned above. In principle, direct methane formation could first occur *via* $C + 4H \leftrightarrow CH_4$. However, the equilibrium of this reaction is on the left-hand side at $T > 585$ °C. Consequently, such methane peaks are only observed in the temperature range of 550 °C to 600 °C as a reaction of pure carbon[12] under H_2 or at very high organic carbon contents, such as those occurring in the post debinding of metal injection molding components.[13]

In the temperature range from 750 °C to 800 °C, methane formation under a hydrogen atmosphere was also observed during the heat treatment of powder mixtures of iron and master alloys of strong oxide formers, in particular manganese and silicon.[14] Oro *et al.* postulate an internal getter effect in which an oxygen transfer from carbothermally reduced iron to the alloying elements with a higher affinity for oxygen occurs through

$$(x/y)\mathrm{Me} + 2\mathrm{H}_2 + \mathrm{CO} \leftrightarrow \mathrm{CH}_4\mathrm{O} + (1/\mathrm{y})\mathrm{Me}_x\mathrm{O}_y \quad [2]$$

within the internal powder structure of the powder mixture. This reaction leads to decarburization without a significant oxygen reduction in the corresponding temperature range. The authors assume that the getter-effect scenario is limited exclusively to powder mixtures with iron and a master alloy at correspondingly high hydrogen partial pressures.[15] In later studies, this effect was also found at industrially relevant hydrogen contents of 10 pct in the atmosphere.[16]

Such processes result in significant decarburization, which considerably changes the properties of the powder metallurgical components. In the present work, the extent to which the effect of decarburization by methanation under a pure hydrogen atmosphere also plays a role in pre-alloyed commercially available powders is investigated. In addition, influences of the alloy composition on the delubrication and reduction behavior are studied with an *in situ* gas phase analysis.

II. EXPERIMENTAL

The samples used in the experiment were prepared by various pre-alloyed powders (Höganäs AB, Sweden) with particle sizes of < 150 μm. As a reference, unalloyed steel was chosen. The chemical compositions of the powders are listed in Table I. The lubricant used was an ethylenebisstearamide EBS microwax binder (Deurex AG, Germany). The powders and binder (1.5 wt pct) were mixed and then pressed in cylindrical geometry with a diameter of 28 mm and a height of 6 mm with a pressing force of 600 MPa.

The delubrication and sintering of the samples were carried out in a tube furnace with an inner diameter of 105 mm and a length of 1600 mm. As a protective atmosphere, pure H_2 5.0 (Linde AG, Germany) with a flow rate of 2.5 L/min in atmospheric pressure was used. The water content is specified as 5 ppm by the manufacturer, which equals a dew point of − 65 °C.

Table I. Element Composition and Green Density of the Tested PM Steel Alloys

	Element Content (m Pct)							
	C	Cr	Mn	Cu	Si	P	Mo	Green Density (g/cm^3)
Sint D35	0.2		0.3	0.5		0.45		6.8
Astaloy CrL	0.8	1.5					0.2	6.98
Astaloy CrM	0.8	2.85	0.08		0.5		0.5	6.9
AHC	0.4	1.24	1.41					7.1
85Mo	0.4	1.24	1.33				0.85	7.2
Mild Steel	0.15		0.18					

As the water can remain in the furnace, the upper limit for the dew point is the cumulative amount of water calculated from a heat treatment time of 12 hours, the above-mentioned gas flow, and the furnace volume of 13.9 L, resulting in a cumulative concentration of 7.2 ppm. This equals a dew point of – 25 °C. In this environment, the samples firstly were heated to 450 °C with a dwell time of 10 minutes, and subsequently heated to 1250 °C with a dwell time of 30 minutes. The heating rate was each 3 K/min.

In order to observe the gas composition during the process, *in situ* gas phase observation was carried out by Fourier-transform infrared spectroscopy (FTIR), using a ThermoFisher Scientific Antaris IGS. In this system, the infrared beam from the broadband IR source first passes through a mirror system and enters the tube furnace *via* KBr windows. In the furnace, the beam runs a few millimeters above the samples, leaves the furnace again on the other side of the tube through a KBr window, and is then fed to an external mercury–cadmium–telluride photodetector, where the measuring signal is recorded.

In order to identify single species, reference spectra (CO, CO_2, CH_4) were taken with the help of gas-filled reference cells. During the heat treatment, spectra were taken in temperature steps of 5 K. Each spectrum was analyzed with regard to the detected species. Every species exhibits a characteristic band, whose shape changes with the temperature due to Doppler broadening. Thus, to determine relative concentration of the observed species, a baseline was drawn between two defined fixed points and integrating the area between the baseline and the measured absorbance. For detection of CO, this integration was done between 2120.35 and 2118.0 cm^{-1}, CO_2 was determined between 2331.32 and 2332.82 cm^{-1}, CH_4 between 3085.33 and 3086.18 cm^{-1}, and the CH group between 2834.85 and 2990.61 cm^{-1}. Furthermore the absorbance due to water has been quantified between 3890.59 and 3892.49 cm^{-1}. This method may be defective to some extent due to overlapping effects, but the drawback was accepted due to practicability and better visibility of the results.

Prior to the measurements, a heat treatment cycle was carried out under hydrogen without a load in order to clean the furnace and rule out contamination from residues of previous heat treatments. In addition, thermogravimetric analysis was carried out using a Netzsch STA 409 C equipment. Here, pure EBS binder was pyrolyzed in N_2–H_2 atmosphere at a heating rate of 5 K/min. The analysis of residual carbon after heat treatment was carried out on a LECO CS230 instrument.

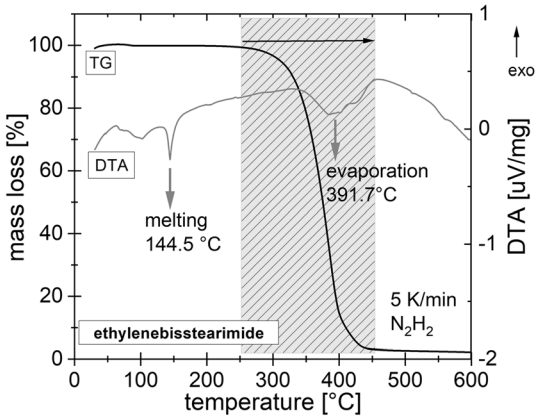

Fig. 1—Thermogravimetric analysis of debinding of the ethylenebisstearamide binder under Ar–H_2 atmosphere. The main debinding step occurs between 336 °C and 408 °C.

III. RESULTS

The result of the thermogravimetric analysis of the ethylenebisstearamide (EBS) is displayed in Figure 1, which shows an onset of the mass loss at temperature range from 250 °C to around 450 °C. Overall, a mass loss of 96.9 pct is measured by the end of the heating phase. In addition, an endothermic peak at 144.5 °C indicates the melting of the EBS binder, and vaporization takes place with a peak at 392 °C.

The Fourier-transform infrared spectrometer flanged to the tube furnace is used to record spectra at various temperatures. For reasons of space, the spectra of all tested alloys and temperatures are not presented here. Figure 2 therefore shows the spectra produced during the heat treatment of the alloy Astaloy CrL at selected temperatures of 360 °C and 385 °C, 770 °C and 875 °C as well as at 1050 °C and 1200 °C. Firstly, a decreasing absorbance from high to low wavenumbers at the lower temperatures catches the eye. This gradient is high at 360 °C and somewhat lower at 385 °C and has its origin in the wavelength-dependent scattering of IR photons on particles. Such particles are formed as soot particles

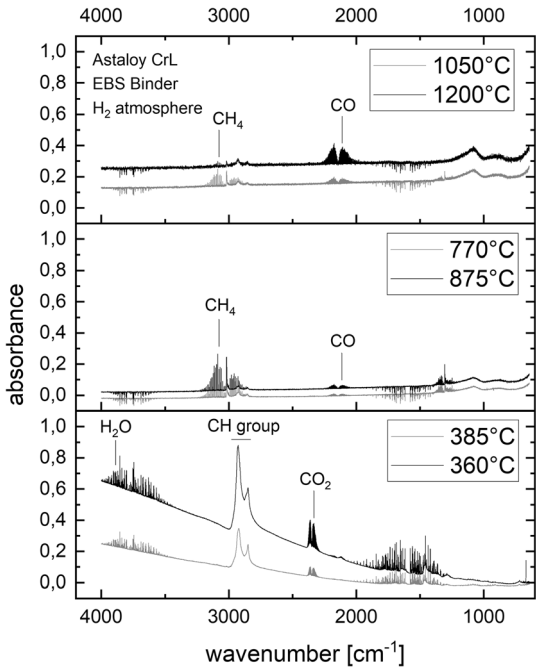

Fig. 2—Typical absorbance spectra of an Astaloy CrL sample during the heat treatment und pure hydrogen. As an example, the spectra at 360 °C, 385 °C, 770 °C, 875 °C, 1050 °C, and 1200 °C are shown. At the typical wavenumbers H_2O-, CH_4-, CO_2-, and CO-absorption peaks are observed. Furthermore, a distinct characteristic CH group absorption peak is measured.

during the decomposition of the EBS binder and indicate a maximum of decomposition activity at 360 °C. At higher temperatures, such a particle-derived scattering is not observed. On the other hand, a rising baseline can be recognized at high temperatures. This is caused by an increasing radiation background due to the heat radiation from the furnace.

Various characteristic peaks can now be detected from the individual spectra. Particularly characteristic is the band between 2700 and 3000 cm^{-1}, which is caused by the absorption of the CH group and also reaches its maximum height at 360 °C, *i.e.*, the temperature of maximum particle formation. Absorption by H_2O molecules is also dominant in this temperature range, covering the characteristic fingerprint range of 1270 to 1900 cm^{-1} and above 3500 cm^{-1}. Furthermore, peaks at wavenumbers of 2120 cm^{-1} indicate the presence of CO, and in the range of 2280 to 2390 cm^{-1} the presence of CO_2 can be read. Finally, peaks in the range of 3085 cm^{-1} at temperatures above 700 °C can be assigned to the formation of CH_4.

From the spectra the integrated absorbance areas in the complete temperature range were calculated. The absorbance of the CH group is depicted in Figure 3(a). In general, the absorbance caused by the CH group is visible in the temperature range of 230 °C to 480 °C, whereby the peak temperatures differ significantly between the individual alloys. As an example, the peak temperature of the chromium and molybdenum containing alloy 85Mo shows a maximum at 330 °C, whereas the absorbance of the CH band of Astaloy CrM is maximal at 368 °C. The maximum absorbance value of all samples is nearly the same.

The formation of CO_2 takes place in parallel with the formation of CH and has maxima between 330 °C and 375 °C (Figure 3(b)). These peak temperatures are equal to the peaks of CH formation with only slight deviations. At higher temperatures no CO_2 formation is visible.

The absorbance caused by CO molecules is displayed in Figure 4(a). Only minor peaks are visible in the above-mentioned temperature range of the maximum EBS binder evaporation. The low carbon-containing mild steel shows no distinct CO formation during the complete heating cycle. At low temperatures, a weak CO formation is detected during heating of the Astaloy steels CrL and CrM and the Sint D35 steel in the temperature range of 335 °C to 370 °C. At higher temperatures, CO formation starts at ~ 770 °C and increases with increasing temperature up to ~ 1050 °C. This is shown by all steel alloys. The formation of strong CO peaks during the heat treatment of CrL and CrM at temperatures > 1000 °C with a maximum in the range of 1200 °C should also be emphasized.

Absorption due to the presence of methane during heating is shown in Figure 4(b). In the lower temperature range at $T < 600$ °C, no significant methane formation is detected in any alloy. In the case of unalloyed steel and Sint D35 with low carbon contents, the methane content remains irrelevant even at higher temperatures. In contrast, the alloys 85Mo and AHC with an carbon content of 0.4 wt pct show a single maximum at 755 °C and 770 °C, respectively. Finally, the alloys CrM and CrL with a high carbon content of 0.8 wt pct each display two methane peaks in the temperature range between 810 °C and 1020 °C.

The absorption due to the formation of H_2O molecules is shown in Figure 5. In general, the formation of H_2O follows the pattern of the formation of CH and CO with peaks in the temperature range of 340 °C and 390 °C. In detail, however, the temperatures of the respective peaks are slightly but significantly higher than those of CH and CO_2 formation. In addition, the range of water formation is wider for unalloyed steel.

Finally, the carbon contents of the samples were determined after the heat treatment. Table II gives the results of the measurements in comparison to the alloy definition carbon content. It appears that all alloys show reduced carbon contents. A particularly high carbon loss was observed in the Astaloy CrL and CrM samples, while the carbon loss in the remaining samples was rather moderate.

IV. DISCUSSION

The heat treatment of ethylenebisstearamide containing PM steels is a complex process that comprises the decomposition of the organic material, as well as deoxidation and decarburization, that occur within several temperature steps. These processes are reflected in events at various temperature ranges. In this sense,

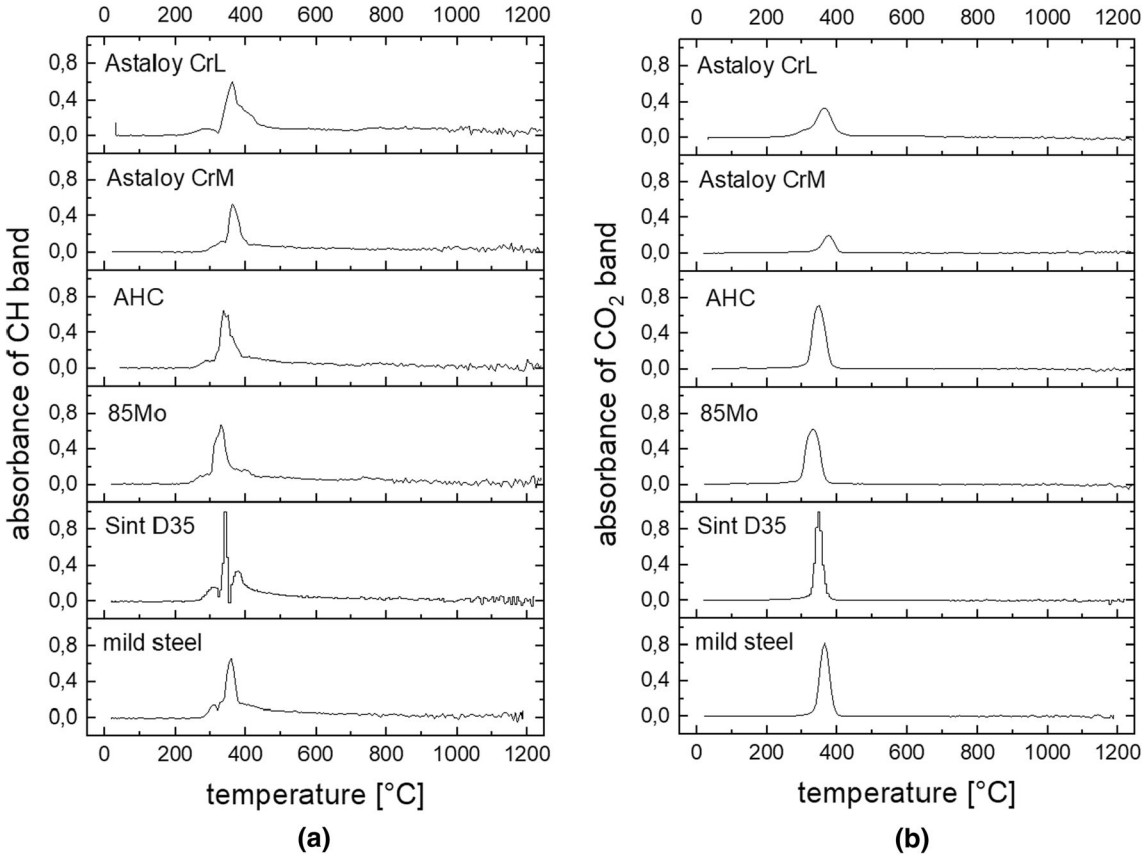

Fig. 3—CH group absorbance (*a*) and CO_2 absorbance (*b*) of various PM steels as a function of temperature under H_2 atmosphere. The release of CH and CO_2 both indicate the main debinding step and occur between 230 °C and 480 °C.

the delubrication of the ethylenebisstearamide (EBS) is attributed to the decomposition of its molecular chains. As reported earlier, the scission of the EBS molecular structure most likely occurs at the carboxylic acid groups. It has been shown that the major decomposition products are CH valence groups.[17] Such species could be expected due to the presence of aliphatic hydrocarbons as one main element in the molecular structure of the EBS chain structure.[5,18] In this case, the process gas atmosphere is the hydrogen source for the molecular chain fragments.

In this way, the delubrication in the present work can be assigned to the occurrence of the CH group at a temperature between 330 °C and 410 °C, at which the thermogravimetric measurement also records a relevant mass loss. The formation of CO_2 is visible parallel to the formation of the CH group. In spite of the fact that other authors have attributed the formation of CO_2 peaks to the decomposition of superficial carbonates and hydrocarbonates,[8] it is therefore more likely that this species is also linked to the delubrication process as a fragment of the decomposition. The same applies to the small CO peaks between 340 °C and 370 °C, which occur at the same temperature as the peaks of the CH group. Like the CH group, CO is also a fragment in the decomposition of ethylenebisstearamide.[5] It is therefore obvious that the formation of CO in this temperature range is caused by the decomposition of the EBS binder and therefore appears at the same time as the CH group.

Both the thermogravimetric measurement and the gas analysis show a single-step decomposition of the EBS binder. The same findings have been reported by Baum *et al.*,[5] who proposed the use of corresponding sensors to monitor the delubrication behavior. Poskrebyshev *et al.* declared the decomposition of EBS in the presence of Fe/C to be triggered by catalytic effects.[19] This catalytic effect can also explain the significant difference between the decomposition temperature of pure EBS binder and the decomposition temperature of EBS-containing steel powder compacts in this study. The former was determined by TGA measurements, while the latter was measured by FTIR analysis of the CH group formed in the furnace. Following this idea, it could now be assumed that the pronounced differences in the peak temperature during the formation of the CH group also result from different alloy compositions and the resulting catalytic effects. However, since the differences of the alloying element concentrations are rather low it is much more likely that the green density plays a more pronounced role during the debinding process. Here, low green densities correlate to higher debinding temperatures. A plausible explanation for this behavior is the thermal conductivity of the green compact, which

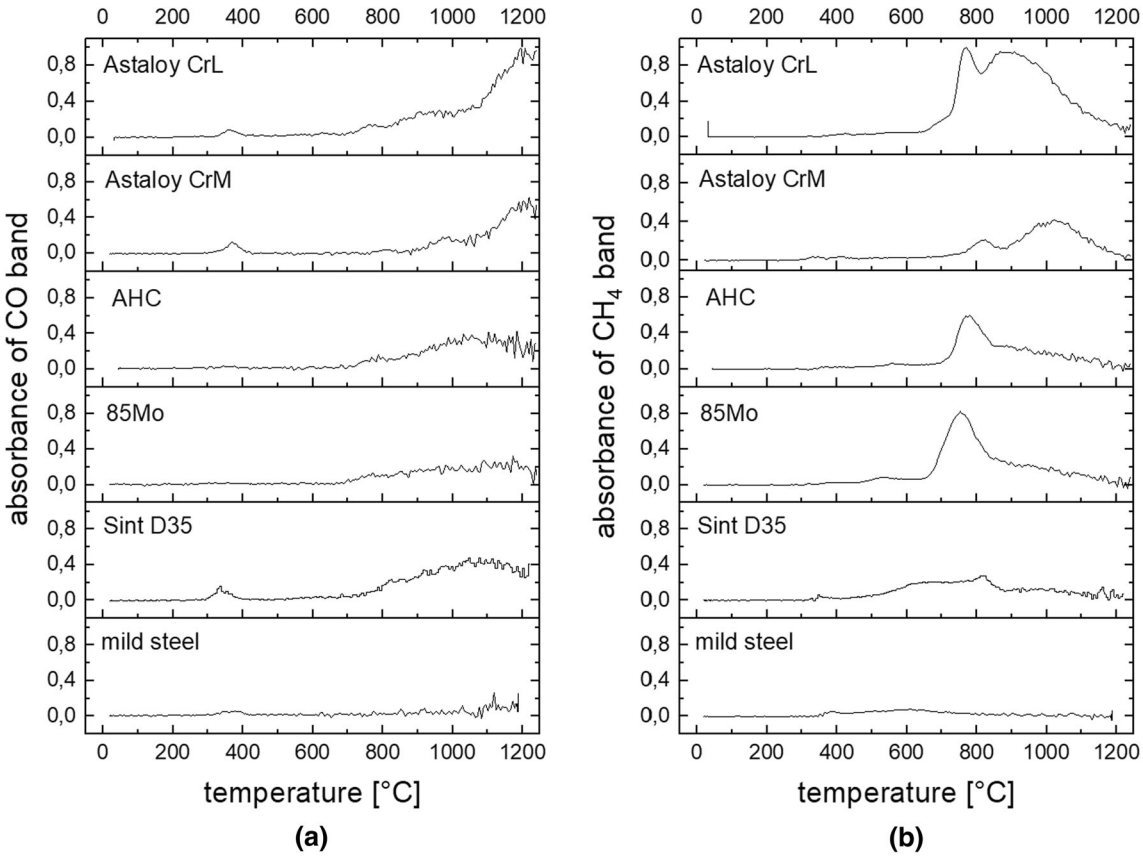

Fig. 4—CO absorbance (*a*) and CH_4 absorbance (*b*) of various PM steels as a function of temperature under H_2 atmosphere. The release of CH_4 at higher temperatures is dependent on the carbon content of the alloy. A significant formation of CH_4 only occurs at carbon contents of > 0.2 wt pct.

increases with green density due to the increasing number of particle contacts. This behavior is immediately apparent and has been demonstrated both experimentally and in models.[20,21] Consequently, the critical temperature for the decomposition of the EBS binder within the powder compact is reached later at lower green densities. Due to the constant heating rate applied in the experiment, the maximum peak formation temperature of the decomposition products appears at higher temperatures.

The measured water formation at temperatures up to 400 °C appears in a similar temperature range to the peaks of CO_2 formation and the formation of the CH group. In detail, however, these peaks differ significantly by several 10 K each. The formation of water can therefore not be attributed to delubrication, but to a reduction *via*

$$\frac{2}{n}\mathrm{M}_m\mathrm{O}_n + 2\mathrm{H}_2 \leftrightarrow \frac{2m}{n}\mathrm{M} + 2\mathrm{H}_2\mathrm{O}. \qquad [3]$$

Typically, around 50 pct of the oxides are removed by this reaction.[22] The partial pressure ratio of H_2 and H_2O, which is linked to the dew point, is the decisive factor for the reduction. With the dew point calculated above at − 25 °C, an equilibrium on the right-hand side of (1) is obtained by plotting the Ellingham diagram from temperatures of around 200 °C. Due to the temperatures of the first occurrence of H_2O, which are on average about 150 K higher, it can be assumed that the dew point during the measurements is somewhat higher in practice, which can be caused by adsorption on the furnace surfaces. Danninger *et al*. report water peaks at around 350 °C when measuring Fe0.5C and in Fe3Cr0.5Mo0.5C under H_2 and conclude that the reduction of iron oxides is present here.[9] Temperature differences in the measurements of different alloys observed in the present study are therefore less attributable to the different alloying elements, but rather to different dew points during heat treatment (which can occur in the laboratory tube furnace, in particular due to the surface adsorbances mentioned above).

In addition to reduction by water formation, carbothermal reduction plays a decisive role for the material properties after sintering. For these reactions, it is initially useful to consider the carbon activity *a*c. Carbon activity is a thermodynamic parameter that describes the reactivity of carbon. The carbon activity in the unalloyed austenite of pure iron can initially be approximated under the carbon content c_C by the following expression[23]:

$$\log a_c = \frac{2300}{T} - 2.21 + 0.15c_C + \log c_C. \qquad [4]$$

In alloyed austenite, the carbon activity becomes

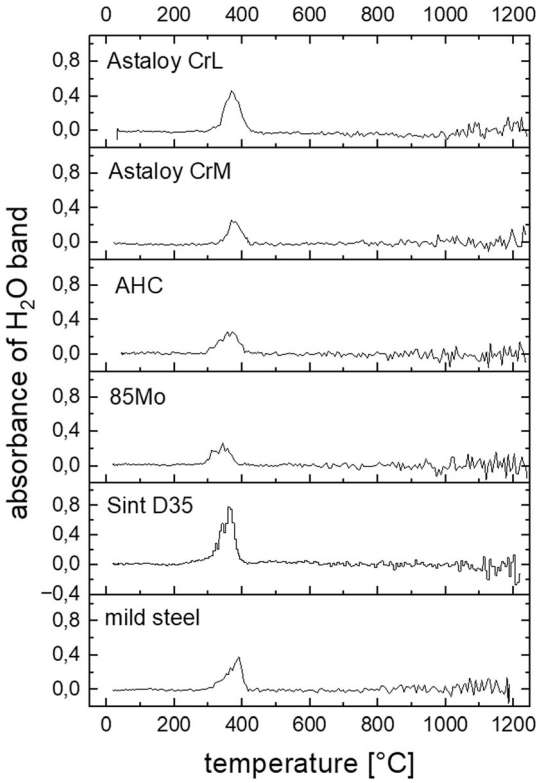

Fig. 5—H_2O absorbance of various PM steels as a function of temperature under H_2 atmosphere. The release of water occurs during the main debinding step.

Table II. Definition of the Carbon Contents of Various PM Steels and Measured Carbon Content After Heat Treatment in H_2 Atmosphere

	Carbon Content (m Pct)	
	After Definition	After Sintering in H_2
Sint D35	0.2	0.08 ± 0.01
Astaloy CrL	0.8	0.46 ± 0.04
Astaloy CrM	0.8	0.45 ± 0.01
AHC	0.4	0.34 ± 0.05
85Mo	0.4	0.34 ± 0.01
Mild Steel	0.15	0.03 ± 0.02

A distinct carbon loss is observed.

$$a_k = f \cdot a_c. \quad [5]$$

The factor f expresses the additive effects of various impurities and alloying elements on the activity of carbon in austenite and can be written numerically as follows[23]:

$$\log f = c_{Si} \cdot 0.055 - c_{Mn} \cdot 0.016 - c_{Cr} \cdot 0.043 - c_{Mo} \cdot 0.015 - c_{Cu} \cdot 0.006. \quad [6]$$

Here, c_{Si}, c_{Mn}, c_{Cr}, c_{Mo}, and c_{Cu} are the percentage contents of the respective alloy elements.

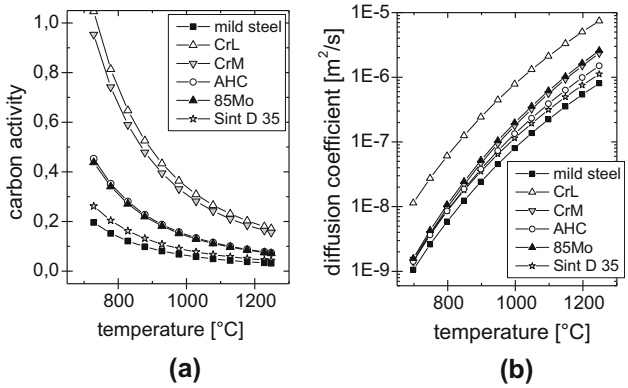

Fig. 6—Calculation of the carbon activity (*a*) and of the diffusion coefficient (*b*) of various PM steel alloys. The formation of methane at higher temperatures is inhibited by decreasing carbon activity and promoted by increasing diffusion coefficients.

The temperature-dependent calculation result for the corrected carbon activity of the alloys considered in this study is illustrated in Figure 6(a). The figure shows that, on the one hand, the reactivity of the carbon decreases with temperature for all alloys. However, it also shows that this carbon reactivity is highest for the alloy CrL and CrM, and decreases in descending order *via* AHC, 85Mo, Sint D35, and mild steel. This order correlates with the decrease in carbon content after sintering, *i.e.*, with high carbon losses in CrL and CrM and somewhat smaller changes in 85Mo and AHC. Such a decarburizing effect is initially achieved by delubrication.

On the other hand, at lower temperature the carbon availability mainly is limited by its diffusivity. The carbon diffusivity D of an alloy with the carbon content c_C can be calculated *via*[24]

$$D = D_0 \exp\left(-Q \cdot 4.1868 \cdot (R \cdot T)^{-1}\right), \quad [7]$$

where R is the gas constant and

$$Q = 36{,}667 - 8862 \cdot c_C + 250 \cdot c_{Mn} + 2950 \cdot c_{Cr} + 2722 \cdot c_{Mo} + 406 \cdot c_{Si}, \quad [8]$$

$$D_0 = 0.039925 + 0.3738 \cdot c_C + 0.014 \cdot c_{Mn} + 0.095 \cdot c_{Cr} + 1.026 \cdot c_{Mo} + 0.0444 \cdot c_{Si}. \quad [9]$$

The calculated carbon diffusivity is shown in Figure 6(b) as a function of temperature. In general, the diffusivity increases with increasing temperature. With respect to the alloy composition, the values of the carbon activity differ significantly from each other. The figure shows a distinctive ranking of the diffusivity from the highest to the lowest as follows: Astaloy CrL, 85 Mo, Astaloy CrM, AHC, Sint D35, and mild steel. In the upper temperature range, however, the influence of diffusion on the supply of carbon is rather limited, as the diffusion path lengths are rather small due to the small particle sizes. This means that the upper limit of the

carbon availability is rather limited by the total availability, *i.e.*, by the carbon activity. The influence of diffusivity should be particularly relevant toward low temperatures. Here, however, the thermodynamics is more of a limiting factor. This applies in particular to the carbothermal reduction according to Eq. [2], which is limited at low temperatures. Therefore, hardly any alloy-specific effects of diffusivity can be recognized in the present study.

At temperatures below 1000 °C, instead, a noticeable progression of methane concentrations is visible in the present experiments. Direct methanation *via* $C + 4H \leftrightarrow CH_4$, as observed in systems with high carbon contents (such as in metal injection molding or in template-based cellular metals), can be ruled out here for thermodynamic reasons, as the equilibrium of the above reaction is on the left-hand side from $T > 585$ °C onwards. In the present study, however, methane formation takes place at temperatures > 750 °C, *i.e.*, at temperatures that are typical for the carbothermal reduction of surface iron oxides. In the present study, methane peaks only occur in particular in the alloys with a carbon content > 0.4 pct (CrM, CrL, AHC, 85Mo) at temperatures, where CO peak of iron reduction would have been expected.

Based on the internal getter effect in master alloy mixtures postulated by Oro *et al.*,[15] it is plausible to assume on the basis of the available data that such an oxygen transfer to oxygen-sensitive alloying elements also occurs in pre-alloyed powders if the carbon potential is sufficiently high. Initially, a reduction of the iron surfaces *via* $Fe_3O_4 + 4C \leftrightarrow 3Fe + 4CO$ takes place inside the powder structure. As the Boudouard equilibrium above 700 °C is on the CO side, CO_2-based mechanisms hardly contribute to the reduction. According to this model, a reaction of the H_2-protective atmosphere and the released CO with the solid metallic alloy components chromium, manganese, and silicon to methane and the corresponding oxides will take place in the powder bed according to Eq. [2]. For the oxidation of chromium, (2) is thermodynamically possible up to about 950 °C, for manganese and silicon also far above this temperature.[15] This reaction requires a sufficient amount of surface carbon and is only visible if the carbon potential is sufficiently high. Furthermore, it can be assumed that a reduction of superficial chromium oxides at temperatures below 1000 °C also results in an oxygen transfer to the more oxygen-sensitive metals Mn and Si, thereby generating the observed second significant CH_4 peak in the CrL alloy.

In addition it can be assumed that the oxygen transfer can also occur by reduction of the inner iron oxides. Such a reduction typically takes place at temperatures of approx. 1050 °C. According to the model of the internal getter effect, this internal reduction also generates an oxygen transfer to the alloying elements chromium and manganese, which have a higher affinity for oxygen. This is indicated by the formation of CH_4 and can be observed in the alloy CrM by a peak at 1020 °C. A transfer from iron oxides to chromium oxides is unlikely due to the above-mentioned thermodynamic reasons. In addition to the dominant CH_4 formation, a weak but significant CO formation is recognizable in all alloys in the temperature range of the internal reduction. We therefore assume that CO formed during the internal reduction of iron oxides is only partially converted into CH_4 due to the effect of the internal oxygen transfer. This means that the internal getter effect at this point requires a sufficiently high carbon activity.

This in turn means that the release of CO observed in these two alloys at $T > 1100$ °C is not an indication of a reduction of internal iron oxides, as is the case under inert conditions or under inert gas with reduced H_2 partial pressure. Rather, it can be assumed that these maxima are caused by the reduction of the oxides of the alloying elements chromium and manganese. The results of Danninger *et al.*, who show CO peaks at 800 °C, 1000 °C, and 1200 °C for the alloy CrM under an inert atmosphere, are consistent with these observations.[9]

V. CONCLUSION

The present study investigates the delubrication, reduction, and decarburization of powder metallurgical components based on commercially available pre-alloyed steel powders with ethylenebisstearamide (EBS) as lubricant. An FTIR *in situ* gas phase analysis of the process gas atmosphere during heat treatment prior to sintering under 100 pct hydrogen atmosphere shows the following main results:

It has been shown that EBS in steel components decomposes mainly in the CH group, CO, CO_2, H_2O, and CH_4. Due to their central position in the molecular chain of EBS, the CH group is the dominating species in the spectra of the process gas. Decomposition is detected within the temperature range 230 °C to 480 °C, whereby measurable differences in decomposition temperatures occur between the individual alloys.

Instead of the typical CO release due to the carbothermal reduction of surface iron oxides, methane is detected in components with carbon contents > 0.4 pct in the temperature range from 750 °C upwards. It is assumed that the carbothermal reduction of surface iron oxides leads to an oxygen transfer to the oxygen-sensitive alloying elements. This ''internal getter effect'' has previously been postulated for mixtures of iron powder and master alloy powder and, according to the results available, apparently also occurs with pre-alloyed powders under a pure hydrogen atmosphere.

With a sufficiently high carbon activity, such an internal gettering effect also occurs during the reduction of superficial chromium oxides, leading to oxygen transfer to more oxygen-sensitive alloying elements. In the same way, the reduction of internal iron oxides leads to an internal getter effect. For this reason, a pronounced reduction of the alloying elements chromium, manganese, and silicon can be measured in the temperature range > 1100 °C for alloys with a high carbon content of 0.8 pct. These processes manifest themselves in the formation of intense CO peaks in this temperature range.

Overall, the study shows that the decarburization of powder metallurgical components during the heat treatment phases prior to sintering in a 100 pct hydrogen atmosphere is less due to the mechanism of delubrication, but rather to mechanisms of carbothermal reduction. The alloy composition primarily influences the carbon activity. Depending on this carbon activity, carbothermal reduction manifest themselves in methane formation in the range from 700 °C to 1000 °C and in carbon monoxide formation above this temperature.

ACKNOWLEDGMENTS

The authors are grateful to the German Ministry for Education and Research (BMBF) for funding (Grant No. 03WKB06C).

CONFLICT OF INTEREST

The authors declare to have no conflict of interests.

FUNDING

Open Access funding enabled and organized by Projekt DEAL.

OPEN ACCESS

This article is licensed under a Creative Commons Attribution 4.0 International License, which permits use, sharing, adaptation, distribution and reproduction in any medium or format, as long as you give appropriate credit to the original author(s) and the source, provide a link to the Creative Commons licence, and indicate if changes were made. The images or other third party material in this article are included in the article's Creative Commons licence, unless indicated otherwise in a credit line to the material. If material is not included in the article's Creative Commons licence and your intended use is not permitted by statutory regulation or exceeds the permitted use, you will need to obtain permission directly from the copyright holder. To view a copy of this licence, visit http://creativecommons.org/licenses/by/4.0/.

REFERENCES

1. G. Kalss, C. Gierl-Mayer, H. Danninger, and G. Stetina: *Powder Metall. Prog.*, 2020, vol. 20, pp. 81–93.
2. G.F. Bocchini: *Powder Metall. Prog.*, 2004, vol. 4, pp. 1–34.
3. S. Ray and R.P. Cooney: in *Handbook of Environmental Degradation of Materials*. M. Kutz, ed., William Andrew Publishing, Norwich, 2018, pp. 185–206.
4. K. Pielichowski, J. Njuguna, and T.M. Majka: in *Thermal Degradation of Polymeric Materials*. K. Pielichowski, J. Njuguna, and T.M. Majka, eds., Elsevier, Amsterdam, 2022, pp. 1–9.
5. M.M. Baum, R.M. Becker, A.M. Lappas, J.A. Moss, D. Apelian, D. Saha, and V.A. Kapinus: *Metall. Mater. Trans. B*, 2004, vol. 35B, pp. 381–92.
6. S. Karamchedu, E. Hryha, and L. Nyborg: *Mater. Process. Technol.*, 2015, vol. 223, pp. 171–85.
7. E. Hryha and J. Wendel: *J. Am. Ceram. Soc.*, 2018, vol. 102, pp. 748–56.
8. E. Hryha, E. Dudrova, and L. Nyborg: *J. Mater. Process. Technol.*, 2012, vol. 212, pp. 977–87.
9. H. Danninger and C. Gierl: *Sci. Sinter.*, 2008, vol. 40, pp. 33–46.
10. R. de Oro Calderon, C. Gierl-Mayer, and H. Danninger: *J. Therm. Anal. Calorim.*, 2017, vol. 127, pp. 91–105.
11. T. Mori, J. Yang, and M. Kuwabara: *ISIJ Int.*, 2007, vol. 47, pp. 1387–93.
12. A. Kirchner, K. Eymann, P. Quadbeck, A. Strauß, and B. Kieback: *MRS Proc. Libr.*, 2013, vol. 1526, p. 707.
13. P. Quadbeck, A. Strauß, and B. Kieback: *Proceedings of WorldPM 2016*, 2016, Hamburg, Shrewsbury. ISBN 987-1-899072-48-4.
14. H. Danninger, A. Avakemian, C. Gierl-Mayer, M. Dlapka, and M. Grafinger: *Proceedings of EuroPM 2014*, 2014, Paper-Nr. 7 O4 EP14038.
15. R. Oro, M. Campos, C. Gierl-Mayer, H. Danninger, and J.M. Torralba: *Metall. Mater. Trans. A*, 2015, vol. 46A, pp. 1349–59.
16. S. Geroldinger, M. Hojati, C. Gierl-Mayer, H. Danninger, and R. Hellein: *HTM J. Heat Treat. Mater.*, 2024, vol. 79, pp. 147–58.
17. P. Quadbeck, A. Strauß, S. Müller, and B. Kieback: *J. Mater. Process. Technol.*, 2016, vol. 231, pp. 406–11.
18. S. Karamchedu, E. Hryha, and L. Nyborg: *Powder Metall. Prog.*, 2011, vol. 11, pp. 90–96.
19. G.A. Poskrebyshev, M.M. Baum, J.A. Moss, and D. Apelian: *Appl. Catal. A*, 2007, vol. 327, pp. 52–65.
20. O.M. Ibrahim, A.J. Al-Saiafi, and S. Alotaibi: *Heat Mass Transf.*, 2021, vol. 57, pp. 1289–1304.
21. J.M. Montes, E.G. Cuevas, J. Cintas, and O. Urban: *Appl. Phys. A*, 2011, vol. 105, pp. 935–47.
22. E. Hryha, L. Nyborg, A. Malas, S. Wiberg, and S. Berg: *Powder Metall.*, 2013, vol. 56, pp. 5–10.
23. M.G. Skalecki, H. Klümper-Westkamp, M. Steinbacher, and H.W. Zoch: *HTM J. Heat Treat. Mater.*, 2018, vol. 73, pp. 80–95.
24. R. Bernst and H.-J. Eckstein (Ed.): *Technologie der Wärmebehandlung von Stahl*, Dt. Verl. für Grundstoffindustrie, 1987, p. 469. ISBN-13 9783342002208.

Publisher's Note Springer Nature remains neutral with regard to jurisdictional claims in published maps and institutional affiliations.